Author Manuscript

Biodegradable Honeycomb-Mimic Scaffolds Consisting of Nanofibrous Walls

Young Gun Ko, Laura A. Smith Callahan, and Peter X. Ma**

Y. G. Ko

Department of Chemical Engineering and Materials Science

Sangmyung University

Hongjimun 2-gil 20, Jongno-gu, Seoul 03016, Republic of Korea

E-mail: younggun@smu.ac.kr

L. A. Smith Callahan, P. X. Ma

Department of Biomedical Engineering

University of Michigan

Ann Arbor, MI 48109, USA

P. X. Ma

Department of Biologic and Materials Sciences

University of Michigan

Ann Arbor, MI 48109, USA

This is the author manuscript accepted for publication and has undergone full peer review but has not been through the copyediting, typesetting, pagination and proofreading process, which may lead to differences between this version and the Version of Record. Please cite this article as doi: 10.1002/mabi.202300540.

This article is protected by copyright. All rights reserved.

E-mail: mapx@umich.edu

P. X. Ma

Macromolecular Science and Engineering Center

University of Michigan

Ann Arbor, MI 48109, USA

P. X. Ma

Department of Materials Science and Engineering

University of Michigan

Ann Arbor, MI 48109, USA

Author Manuscript

Keywords: polymeric biomaterials, biomimetic honeycomb, phase separation, nanofibrous scaffolds, tissue engineering

The scaffold is a porous three-dimensional (3D) material that supports cell growth and tissue regeneration. Such 3D structures should be generated with simple techniques and nontoxic ingredients to mimic bio-environment and facilitate tissue regeneration. In this work, we demonstrate simple but powerful techniques for the fabrication of lamellar and honeycomb-mimic scaffolds with poly(L-lactic acid). The honeycomb-mimic scaffolds with tunable pore size ranging from 70 to 160 μm are fabricated by crystal needle-guided thermally induced phase separation in a directional freezing apparatus. The compressive modulus of the honeycomb-mimic scaffold is ca. 4

This article is protected by copyright. All rights reserved.

times higher than that of scaffold with randomly oriented pore structure. The fabricated honeycomb-mimic scaffold exhibited a hierarchical structure from nano-fibers to micro-/macro-tubular structures. Pre-osteoblast MC3T3-E1 cells cultured on the honeycomb-mimic nanofibrous scaffolds exhibit an enhanced osteoblastic phenotype, with elevated expression levels of osteogenic marker genes, than those on either porous lamellar scaffolds or porous scaffolds with randomly oriented pores. The advanced techniques for the fabrication of the honeycomb-mimic structure may potentially be used for a wide variety of advanced functional materials.

Author Manuscript

1. Introduction

Since tissue engineering came into the spotlight for the repair and regeneration of defective organs and tissues,[1] various scaffolds mimicking the natural extracellular matrix have been developed to create the optimum environment for cell adhesion, growth, migration and differentiation.[2,3] To maximize the performance of these scaffolds, complex three-dimensional (3D) structures need to be generated with simple techniques and biocompatible ingredients.[4] Many tissues such as nerve, ligament, tendon, muscle, dentin, and bone have anisotropic architectures. We hypothesized that a scaffold with honeycomb-mimic oriented tubular pores would promote anisotropic tissue regeneration and function. Honeycomb structure with oriented pores is highly represented in nature such as in whale baleen,[5] compact bone,[6] cedar, grass stems, a feather rachis,[7] and so forth. These natural materials possess excellent mechanical properties due to their capacity in energy dissipation from nano-scale[8] to macro-scale.[9] For example, honeycomb micro-composites have been reported to possess a high ratio of strength to weight.[10] Poly(L-lactic acid) (PLLA) scaffolds with oriented tubular pores were previously fabricated using a directional temperature gradient.[11] However, the method has limited control over the tubular diameter. PLLA is one of the best biodegradable polymers for the medical applications owing to the its biocompatibility and mechanical strength. The United States Food and Drug Administration (FDA) approval for its medical applications was granted in 1996.[12]

This article is protected by copyright. All rights reserved.

The fabrication of tubular structures with the unidirectional-freezing technique have been studied and attempted using various materials[13] such as NiO composites,[14] gelatin composites,[15] fibrous protein with a polysaccharide,[16] graphene aerogels,[17] kapok fibers/sodium alginate suspensions,[18] ceramic nanofibers,[19] etc. The fabricated honeycomb structure exhibited high strength. This structure provides directional cell migration and growth for the tissue regeneration. Cells are inherently sensitive to physical biochemical, and chemical stimuli from their surroundings.[20] Surface topography is an important factor in those stimuli, and serves positive stimuli to cells for adhesion, growth, differentiation, and so on.[21] The wall surface of the honeycomb-mimic structure is nearly smooth. Therefore, the effect of the surface topography to cells may not be expected. Hu et al. fabricated the honeycomb monolith structured porous PLLA by unidirectional freezing and freeze-drying.[22] Poly(ethylene glycol) was used to create pores in the microtube walls in the honeycomb monolith structure. However, the pores were not created finely.

In this study, we developed techniques to fabricate lamellar and honeycomb-mimic PLLA scaffolds by crystal needle-guided thermally induced phase separation (TIPS) in a directional freezing apparatus. Biodegradable and biocompatible PLLA scaffolds with adjustable tubular pore diameter and nanofibrous pore walls were finely generated from PLLA, dimethyl carbonate (DMC), and *p*-aminobenzoic acid (PABA), which are all nontoxic materials.[23-25] The concept for design of the honeycomb-mimic scaffolds consisting of nanofibrous walls promotes mechanical properties of scaffolds and cellular behavior of transplanted cells (cell adhesion, proliferation, and differentiation) using vertical wall, surface roughness, and nano-fibrous structures.[26-30] The pore-oriented PLLA scaffolds with various wall textures were also prepared using the co-solvent system and the directional freezing apparatus.

2. Results and Discussion

2.1. Thermally Induced Directional Phase Separation

This article is protected by copyright. All rights reserved.

Author Manuscript

The PLLA/DMC solution was phase-separated at a suitable low temperature, and the crystallized DMC was then removed by sublimation to generate the porous PLLA scaffolds. When the PLLA scaffolds were fabricated using a phase-separation temperature of -20 ^{o}C without directional freezing, the pores in the PLLA scaffolds were randomly oriented due to the lack of uniaxial temperature gradient (**Figure 1**a). The oriented pore architecture in the scaffolds was achieved by freezing the PTFE mold filled with PLLA/DMC solution between two metal rods whose temperatures were individually controlled by a computer using liquid nitrogen and heating tapes (Figure 1b). To ensure the heat conductivity and cooling direction from the bottom to the top of the mold, stainless steel caps were used as the top and bottom covers of the PTFE mold, which were in contact with the top and bottom rods at two different temperatures (the bottom was at a lower temperature than the top) for the directional freezing along the vertical axis. The side of the cylindrical PTFE mold was surrounded with insulating styrofoam. Phase-separation of the PLLA solution was carried out at a cooling rate of -0.25 ^{o}C min^{-1}, -0.5 ^{o}C min^{-1}, or -1 ^{o}C min^{-1} (Figure 1c). The difference between the actual and the set temperatures was always maintained to be smaller than 0.7 ^{o}C. While the pores in the PLLA scaffolds fabricated at -20 ^{o}C in a freezer were randomly oriented, the PLLA scaffolds fabricated with the directional freezing apparatus showed a layered architecture (Figure 1d). The pore architecture was controlled by the crystal shape of the solvent in the solid-liquid phase-separation process likely because the solvent crystal growth concentrated the polymer to form the pore walls. The shape of the DMC crystals formed by freezing is plate-like (Figure 1e). The image of the DMC crystal growth was obtained by freezing the DMC vapor on a cold tungsten wire that served as the condensation surface for the forming DMC crystals in the chamber (Movie S1, Supporting Information). During the freezing of the PLLA/DMC solution by the directional freezing apparatus, the concentrating PLLA was entrapped between plate-like DMC crystals that grew from the bottom to the top of the mold. After sublimation to remove the DMC crystals grown out of the PLLA/DMC solution in the directional freezing apparatus, layered polymer architecture was formed, which may not be ideal for a tissue-engineering scaffold due to the low structural stability and poor mechanical properties.

2.2. Hierarchical Structure of Honeycomb-Mimic Scaffolds Fabricated by Crystal Needle Guided Phase Separation

This article is protected by copyright. All rights reserved.

Author Manuscript

We hypothesized that the use of a suitable substrate might serve as a nucleating surface that could guide the crystal growth and therefore to control the pore architecture. PABA crystallizes in two different polymorphic forms (the α-polymorph and the β-polymorph).[31] The α-polymorph has needle-like crystals whose structure is consisted of orthorhombic unit cells and monoclinic unit cells (ratio=1:1). The long rectangular side of needle-like crystal (with a cross-section of parallelogram) of PABA could serve as a substrate for DMC crystal growth. Oriented and aligned α-polymorph crystals with the needle-like shape were successfully grown in PABA/DMC solution by the directional freezing apparatus in our previous study.[32]

After dissolving PABA into the PLLA/DMC solution in the mold, the mold was frozen from the bottom to the top with the designed freezing apparatus. This strategy successfully initiated the nucleation from the bottom, the directional growth of the needle-like PABA crystals, and the induced DMC crystal growth. The frozen samples were then freeze-dried to sublimate DMC. The PABA in the sample was leached out with ethanol thereafter. The resulting scaffold had tubular pores, which mimic the architecture of a honeycomb (**Figure 2**a,c,d). During the formation of tubular structure in the scaffold, nano- and micro-sized pores were formed in the walls of tubules (Figure 2b). These pores are advantageous in a scaffold because they may serve as pathways for nutrients and signaling molecules as well as possible interactions between cells that attach on the two opposite sides of the wall. Larger micro pores may also pave the way for the formation of vessels through the tubular walls similar to those in the compact bone.[33]

Without PABA, the PLLA in the PLLA/DMC solution was concentrated between the growing DMC crystal layers during the freezing process to form the layered architecture in the porous polymer scaffold. Similar layered ceramic structure was created when an aqueous suspension of ceramic particles was directionally frozen.[13] In our polymer solution, we added the third component – PABA in the organic solvent in this work. After PLLA/PABA/DMC solution was frozen in the directional freezing apparatus, PABA crystals were observed in the PLLA walls before being leached out (**Figure 3**a). One side of needle-like PABA crystals was exposed. After the PABA crystals were leached out using ethanol, vestiges left behind by the PABA crystals were observed (Figure 3b). To confirm that the needle-like PABA crystals were responsible for the formation of the tubular architecture, we added glass fibers instead of in situ grown needle-like PABA crystals in the PLLA/DMC solution to fabricate the scaffold. The glass fibers were inserted into the mold vertically, and the PLLA/DMC solution was poured into the mold. After freezing the mold using the directional freezing apparatus

This article is protected by copyright. All rights reserved.

Author Manuscript

and the removal of DMC from the mold by freeze-drying, most of the glass fibers were observed between PLLA walls, not in the PLLA walls (Figure 3c). These results demonstrated that the pre-added glass fibers were not a suitable substrate to guide the formation of intersecting DMC crystals and therefore the tubular PLLA walls during the freezing of the PLLA solution. Whereas the long rectangular side of needle-like PABA crystals served as a suitable substrate to guide the direction of DMC crystal growth, while the curved side of the glass fibers could not. To verify this, scaffolds fabricated at various PLLA concentrations with a fixed PABA concentration were examined (Figure 3d). The formation of PLLA walls occurred on two sides of the PABA crystals, but not on the other sides - presumably the sides of the nucleation and crystal growth of DMC. SEM images show the remaining PLLA walls that were originally sandwiched between DMC crystal layers, which grew along the long rectangular sides of needle-like PABA crystals that have a cross-section of a parallelogram. At a suitable polymer concentration, continuous nano-fibrous PLLA walls were formed connecting adjacent PABA crystals.

The scaffold architecture formation is illustrated in cartoons (**Figure 4**a,b). When PLLA/DMC solution was used to fabricate the lamellar PLLA scaffolds, the DMC should have nucleated on the bottom of the mold and the plate-like crystals grew along the freezing direction to the top of the mold, resulting in the formation of layered PLLA walls that were originally sandwiched between DMC crystals (Figure 4a). However, the existence of PABA in the PLLA/DMC solution should have resulted in a two-step crystallization process. Needle-shaped PABA crystals should have formed in the first step prior to the DMC crystallization. These in situ formed PABA crystal needles likely served as the substrate at the bottom of the mold to induce the DMC crystallization along two opposite sides of the PABA fibers as two parallel crystal plates growing from the bottom to the top. The growth of the two crystallized DMC plates on the two opposite sides of a PABA crystal needle concentrated the PLLA in between (Figure 4b). This process led to the formation of a PLLA wall along the freezing direction (vertical direction). The PLLA wall met with another PLLA wall or a needle-like PABA crystal, leading to the formation of a corner edge of a tubule along the freezing direction. Due to the growth of many PABA needles and therefore many PLLA walls, honeycomb PLLA tubules were formed (Figure 4b). Interestingly, at the right conditions, the concentrated PLLA solution could phase separate to form further fine architectural features such as micro/nano pores and nanofibers on the walls. Thus fabricated honeycomb-mimic scaffolds have a hierarchical architecture from nano- to macro-scale. PLLA nanofibers make up the walls of the microtubules, and the microtubules make up the honeycomb-mimic scaffold with the size of millimeters, centimeters, or even a larger scale. This

This article is protected by copyright. All rights reserved.

Author Manuscript

hierarchical architecture resembles certain important architectural features of bone.[2021] The tubules mimic the outer shape of osteons, while PLLA nanofibers mimic collagen fibers.

2.3. Control of Tubular Diameter of Honeycomb-Mimic Scaffolds and The Mechanical Properties

Tubular or fibrous bundle structures in various tissues and organs have different diameters to perform their characteristic functions. For examples, osteons in the compact bone have a tubular diameter of ca. 90 ~ 260 μm,[34] while skeletal muscle fibers have a diameter of ca. 5 ~100 μm.[35] Here we demonstrate the feasibility of regulating the diameter of the tubular pores in the scaffold by varying PLLA and PABA concentrations. High PLLA and PABA concentrations result in a small tubular diameter in the scaffold (**Figure 5**a). While the thickness of pore walls in the scaffolds with randomly oriented pores increased with the PLLA concentration, the pore wall thickness in the lamellar scaffolds and the honeycomb-mimic scaffolds were essentially the same (ca. 2 μm) irrespective of PLLA and PABA concentration. In the case of high PABA concentration, more PABA crystals were formed to induce the formation of more plate-like PLLA walls, leading to a smaller average tubular diameter. At a higher PLLA concentration, more PLLA walls were formed because their wall thickness was essentially the same irrespective of PLLA concentration, leading to a smaller average diameter of the tubules in the scaffold.

We can also vary the cooling rate to vary the tubular diameters in the honeycomb-mimic scaffolds (Figure 5b). A slower cooling rate may allow fewer nuclei to form, resulting in growth of the DMC crystals of larger cross sectional areas. After freeze-drying, the spaces originally occupied by the DMC crystals become the pores in the scaffold. Therefore, the slower cooling rate resulted in larger pores in the scaffold. In this study, the various tubular diameters of 70 ~ 160 μm were successfully generated to mimic the osteon size in the compact bone by controlling the PLLA concentration, PABA concentration, and the cooling rate.

In tissue engineering applications, a biomimetic pore morphology and good mechanical properties of the scaffolds are desired for optimal support of tissue regeneration.[16] Human compact bone is a typical example that exhibits a rich hierarchical structure from collagen fibrils to osteons.[36] Oriented hierarchical structures show high mechanical strength.[37] Although PLLA is biodegradable and

This article is protected by copyright. All rights reserved.

Author Manuscript

biocompatible, highly porous scaffolds in general are mechanically weak. Therefore, a scaffold structure that can improve its mechanical strength is desired for various tissue engineering applications. Scaffolds with a well-defined interconnected spherical pore network are well known to allow efficient cell seeding and can be fabricated into complex shapes.[38] However, such scaffolds do not guide oriented hierarchical tissue structure regeneration. In contrast, lamellar or honeycomb-mimic structures can be designed into uniaxially oriented hierarchical structure, which may guide the directional cell migration, growth, and biomineralization of the organic matrix (and the scaffold).

The compressive modulus of the honeycomb-mimic scaffold was higher than those of scaffolds with lamellar or randomly oriented pore structure. The modulus increased with increasing PLLA concentration (**Figure 6**a). A noteworthy result is that the honeycomb-mimic scaffold fabricated with 2.5% (w v^{-1}) PABA shows higher compressive modulus than that fabricated with 1% (w v^{-1}) PABA at the same PLLA concentration. Higher PLLA and PABA concentrations resulted in formation of more oriented tubules with smaller diameters in the scaffold (Figure 5a). A higher PLLA concentration would result in a lower porosity of the scaffold, which should contribute to the higher modulus. PABA concentration does not contribute to the composition of the final scaffold because it has been leached out by ethanol, but it does contribute to the architectuer of the scaffold. When the PABA concentration is higher while PLLA concentration is the same, the resulting more oriented smaller tubular walls may be able to resist a higher loading for the same amount of deformation. A similar relationship between bone fracture energy and osteon diameter has previously been reported by other research groups: bone having more osteons with smaller diameters exhibited higher strength.[39,40] The compressive modulus of the scaffolds increased exponentially with the increase of the PLLA concentration while it increased linearly with the increase of the cooling rate (Figure 6b). The compressive modulus of the scaffold fabricated at the low cooling rate was low (Figure 5b) likely due to the less oriented tubular pores and the larger diameter of the pores.

2.4. Cell Culture Studies of Honeycomb-Mimic Scaffolds

In tissue development and regeneration, cell-matrix interactions are very important. Biophysical extracellular matrix (such as collagen, fibronectin, vitronectin, fibrillin, GAGs, etc.) and biochemical signals (such as growth factors, cytokines, chemokines, etc.) are transmitted from the

This article is protected by copyright. All rights reserved.

Author Manuscript

microenvironment to cells. These signals influence the gene expression, and cause cells to differentiate, proliferate, migrate, or apoptosis[41] The collagen-mimic nanofibers have been previously developed[42,43] and reported to enhance osteogenic differentiation of cells and to promote mineralized tissue formation.[44-48]

To examine cellular response to the different matrix surfaces and pore orientations in vitro, MC3T3 E1 pre-osteoblasts were seeded onto the scaffolds. After 3 days of culture, cells on the tubular PLLA scaffolds (**Figure 7**c) appeared to be more evenly distributed than cells on either the lamellar PLLA scaffolds (Figure 7b) or the PLLA scaffold with randomly oriented pores (Figure 7a). Additionally, there were regions of the PLLA scaffold with randomly oriented pores that did not contain any cells (Figure 7a), indicating that the pore structure did not allow for even cellular seeding as the tubular and lamellar PLLA scaffolds did. After 2 weeks in culture, the uneven cellular seeding on the PLLA scaffolds with randomly oriented pores led to uneven cellular density in the scaffold as shown in Figure 7d. Statistically significantly higher cellular content was observed on the tubular PLLA scaffolds (29.46 ± 0.58 μg scaffold^{-1}) than those scaffolds with randomly oriented pores (24.39 ± 1.09 μg scaffold^{-1}, $p \leq 0.05$) or the lamellar pores (25.61 ± 0.55 μg scaffold^{-1}, $p \leq 0.01$) after 14 days of culture. However, all the scaffold types had similar DNA contents 12 h after cell seeding (data not shown) indicating that the tubular PLLA scaffold better promoted cellular proliferation compared to the other scaffold types. A significant increase in the expression of osteocalcin (Figure 7g) and bone sialoprotein (Figure 7h) was observed in cells cultured on the tubular PLLA scaffold compared to cells cultured on lamellar scaffolds. Cells cultured on the tubular PLLA scaffold also expressed significantly more osteocalcin (Figure 7g) than cells cultured on the PLLA scaffolds with randomly oriented pores. This increase in the expression of differentiation markers on the tubular PLLA scaffolds compared to the other scaffold types may be related to the homogenous cellular distribution throughout the tubular PLLA scaffold due to the initial even cellular seeding and higher cellular density which have been shown to affect differentiation.[49,50] The pore geometry and inter-pore connectivity could also affect cell shape, cell-scaffold, and cell-cell interactions. The shape of this type of cells and their interactions with culture substrate have been found to significantly affect their osteogenic differentiation.[47] Overall, the results indicate that the tubular PLLA scaffold provides a better environment for initial cellular seeding, proliferation and differentiation than either the PLLA scaffold with lamellar pores or the PLLA scaffold with randomly oriented pores for bone tissue regeneration.

This article is protected by copyright. All rights reserved.

Author Manuscript

Author Manuscript

2.5. Preparation of Various Wall Surfaces in Tubular Scaffolds

Surface topography is an important factor in those stimuli, and serves positive stimuli to cells for adhesion, growth, differentiation, and so on.[20] Although the tubular pore guides the direction of cell growth and migration, it cannot influence the cell differentiation, adhesion and growth rate. To prepare the various surface textures of the scaffolds, a co-solvent system was used during the unidirectional TIPS process. In one-solvent system, the PLLA scaffolds fabricated using 1,4-dioxane and dimethyl carbonate (DMC) showed a fishbone-like pore and a layered architecture with a smooth wall, respectively (Figure 1d).[51] The PLLA scaffold fabricated using the DMC/ethanol(EtOH) solvent system exhibited tubular pores with the rough wall surface (**Figure 8**a). The wall in the scaffold consisting of the bundle of nano-fibers was observed (inset in Figure 8a). The bundle of nano-fibers is like a cell which contains well-developed lamellipodia and filopodia. In the case of a DMC/tetrahydrofuran(THF) solvent system, the wall in the scaffold consisted of flakes (Figure 8b). And the flakes were well oriented unidirectionally. The scaffolds fabricated with DMC/1,4-dioxane and 1,4-dioxane/benzene solvent systems showed unidirectionally fibrous textures (Figure 8c,d). The fiber morphology was different each other. The irregularly ripped morphologies for the DMC/1,4-dioxane system and the hemitubular morphology for the 1,4-dioxane/benzene system were observed.

3. Conclusion

In summary, we have demonstrated the fabrication of the honeycomb-mimic PLLA scaffold with the technique of crystal needle guided and thermally induced directional phase-separation. The directional phase-separation was achieved by freezing the mold from bottom to top with accurately programmed temperature profiles. This novel technique overcomes the limitations of the existing solid-liquid phase-separation methods and allows for better control over the pore size, shape,

This article is protected by copyright. All rights reserved.

orientation and the mechanical properties of the scaffolds. The compressive modulus of the honeycomb-mimic scaffold is three times higher than that of the randomly-oriented-porous scaffold. The fabricated honeycomb-mimic scaffolds have a hierarchical architecture with features from nano- to macro-scale, resembling the natural bone architecture (micro tubules to mimic osteons and nanofibers to mimic collagen morphology). PLLA scaffolds consisting of various textures were prepared using the co-solvent system and the unidirectional-freezing apparatus. Interestingly, the wall in the PLLA scaffold consisting of the bundle of nano-fibers was observed in the case of the DMC/EtOH solvent system. The bundle of nano-fibers is like a cell which contains well-developed lamellipodia and filopodia. Cells on the honeycomb-mimic scaffold exhibited an enhanced osteoblastic phenotype, with elevated expression levels of osteogenic marker genes by approximately over 40%. In addition to fabricating scaffolds for tissue engineering, this advanced technique may potentially be used to fabricate various 3D tubular structures for a wide variety of applications.

4. Experimental Section

Materials: For preparing PLLA (inherent viscosity, [η] = 1.6 dL g^{-1}; Boehringer Ingelheim, Germany) solution and PABA (Sigma, Saint Louis) solution, DMC (Aldrich, Milwaukee) was used as a solvent to achieve various concentrations (PLLA solution: 1.0 ~ 5.0% (w v^{-1}); PABA solution: 1.0 ~ 2.5% (w v^{-1})).

Preparation of PLLA Scaffolds with Randomly Oriented Pores: The PTFE mold containing PLLA solution was transferred into a freezer set to -20 °C to induce solid-liquid phase-separation. The phase-separated PLLA/DMC systems were then transferred into a freeze-drying vessel at -5 °C to -10 °C in an ice/salt bath, and freeze-dried under vacuum (pressure lower than 0.5 mmHg) for 2 weeks.

Preparation of Lamellar and Honeycomb-Mimic PLLA Scaffolds: A solution for making an oriented structure was poured into the PTFE mold whose top and bottom caps were made of stainless steel (Figure 1b). The mold was surrounded by the styrofoam insulation and placed between two stainless steel rods. The two rods were immersed in a bath of liquid nitrogen to freeze the mold. The bath of liquid nitrogen was placed in a bath of ethanol to reduce the volatilization of the liquid nitrogen. A

This article is protected by copyright. All rights reserved.

Author Manuscript

computer, proportional–integral–derivative (PID) temperature controllers, and heating tapes were used to control the temperature of the stainless steel rods. The two rods were cooled from room temperature to -20 °C at a predetermined constant cooling rate while the temperature of the top rod was controlled to be 5 °C higher than that of the bottom rod during the cooling process until the temperature of the bottom rod reached -20 °C (Figure 1c). After the phase separation, the samples were transferred into a freeze-drying vessel at -5 °C to -10 °C in an ice/salt bath, and freeze-dried under vacuum (pressure lower than 0.5 mmHg) for 2 weeks to sublimate and remove DMC. When PABA was added in the PLLA solution to fabricate the honeycomb-mimic scaffold, PABA was leached out after the DMC was sublimated. To leach the PABA crystals out, the PLLA scaffold containing PABA crystals was immersed into ethanol with ethanol changed 3 times a day for 2 days. The scaffold was then washed with the distilled deionized water with water changed 3 times during 24 h. After washing, the scaffold was transferred into a freeze-drying vessel at -5 °C to -10 °C in an ice/salt bath, and freeze-dried under vacuum (pressure lower than 0.5 mmHg) for 2 weeks.

The PLLA composite scaffold with glass fibers (Aldrich, Allentown) was fabricated at 2.5% (w v^{-1}) PLLA and 2.5% (w v^{-1}) glass fibers.

Characterizations of PLLA Scaffolds: The morphologies of the oriented structures were examined using a field emission gun scanning electron microscopy (FEG SEM) (XL30FEG, Philips) at 15 kV. The specimens were cut by a razor blade, and the exposed surfaces were examined. For microstructural observation, the specimens were coated with gold using a sputter coater (Desk-II, Denton Vacuum Inc.). The gas pressure was less than 50 mtorr; the current was about 40 mA; and the coating time was 120 s. The elementary map of the patterned cap was obtained by energy dispersive X-ray spectroscopy using an integrated EDAX Phoenix XEDS systemt attached to the FEG SEM. The compressive mechanical properties of the scaffolds were measured using an MTS mechanical tester (Synergie 200, MTS Systems Corporation, Cary). Circular disk specimens with a diameter of 19.0 mm and a thickness of 4.15 mm were compressed with a crosshead speed of 0.5 mm min^{-1}. The load was applied in the direction parallel to the tubular axis. The compressive modulus was determined from the initial linear region of the stress-strain curve.

Cell Culture and Study: MC3T3-E1 cells (clone 26,[38] passage 19) were cultured in ascorbic acid free alpha minimum essential medium (α-MEM) supplemented with 10% FBS, 100 U mL^{-1} penicillin and 100 μg mL^{-1} streptomycin in a humidified incubator at 37 °C with 5% CO_2. The scaffolds (6.0 mm in diameter and 2.5 mm in thickness) were sterilized using ethylene oxide and soaked in a 50:50

This article is protected by copyright. All rights reserved.

Author Manuscript

PBS:ethanol solution for 1 h under reduced pressure to allow the PBS:ethanol solution to penetrate the scaffold. Afterwards, the PBS:ethanol solution was exchanged with PBS 3 times for 30 min each on an orbital shaker (Model 3520, Lab-Line Instruments, Melrose Park, Illinois) at 75 rpm. Scaffolds were washed with complete medium (α-MEM, 10% FBS, 1% antibiotics) twice for 2 h each on an orbital shaker, transferred to custom-built Teflon trays, and seeded with 2×10^6 MC3T3-E1 cells mL^{-1}. For proliferation and differentiation studies, scaffolds were transferred after 48 h into 6-well tissue culture plates containing 3 mL of complete medium, and cultured for pre-determined times. The medium was changed every other day. After 1 week, the medium was supplemented with 50 µg mL^{-1} ascorbic acid and 10 mM β-gycerol phosphate. For proliferation studies, the scaffolds were washed with PBS for 5 min, homogenized with a Tissue-Tearor (BioSpec Products, Inc., Bartlesville, Oklahoma), and the DNA content was determined with a fluorescence assay from Sigma. Total RNA was isolated using an RNeasy Mini Kit (Qiagen, Valcenica, California) according to the manufacturer's protocol after the scaffolds were mechanically homogenized with a Tissue-Tearor. Based on absorbance readings at 260 nm, 1 µg of RNA from each sample was used to make cDNA with TapMan reverse transcription reagents (Applied Biosystems, Foster City, California) on a GeneAmp PCR (Applied Biosystems) with a 10 min incubation at 25 °C, a 30 min reverse transcription at 48 °C and a 5 min inactivation at 95 °C. Real Time PCR was set up using Sybr Green Master Mix (Applied Biosystems) and specific primer sequences for OCN (5' TGACCTCACAGATGCCACG 3' and 5' CTTATTGCCCTCCTGCTTG 3'), BSP (5' GGCCACGCTACTTTCTTTA 3' and 5' AACTATCGCCGTCTCCATT 3') and GAPDH (5' AGGGCATCTTGGGCTACAC 3' and 5' CATACCAGGAAATGAGCTTGA 3') with a 2 min incubation at 50 °C, a 10 min Taq activation at 95 °C, and 40 cycles of denaturation for 15 s at 95 °C followed by an extension for 1 min at 72 °C on an ABI Prism 7500 Real Time PCR system (Applied Biosystems). Target genes were normalized against GAPDH using a relative standard curve. SEM samples were washed with PBS and 0.1 mol cacodylate buffer, then fixed with 2.5% glutaraldehyde in 0.1 mol cacodylate buffer over night. The scaffolds were washed again with 0.1 mol cacodylate buffer and post-fixed in 1% osmium tetroxide for 1 h. The fixed samples were then dehydrated through an ethanol gradient (50%, 70%, 90%, 95%, and 100%) over 3 h and dried with hexamethyldisilazane. Samples were then gold coated and observed using a field-emission gun (FEG) SEM (Philips XL30). Histological samples were fixed in 10% neutral buffered formalin solution (Sigma, Saint Louis), dried through an ethanol gradient, and embedded in paraffin. Embedded samples were cut into 5 µm sections and stained with Hematoxylin and Eosin-Phloxine.

This article is protected by copyright. All rights reserved.

Author Manuscript

Author Manuscript

Supporting Information

Supporting Information is available from the Wiley Online Library or from the author.

Acknowledgements

The authors thank Ely Silk for the supply of the data of DMC crystal growth.

Received: ((will be filled in by the editorial staff))

Revised: ((will be filled in by the editorial staff))

Published online: ((will be filled in by the editorial staff))

References

[1] R. Langer, J. P. Vacanti, *Science* **1993**, *260*, 920.

[2] P. P. Provenzano, *Nat. Mater*. **2020**, *19*, 130.

[3] C. Zhao, S. Tian, Q. Liu, K. Xiu, I. Lei, Z. Wang, P. X. Ma, *Adv. Funct. Mater*. **2020**, *30*, 2000776.

[4] X. Zhang, Y. Li, Y. E. Chen, J. Chen, P. X. Ma, *Nat. Commun*. **2016**, *7*, 10376.

[5] B. Wang, T. N. Sullivan, A. Pissarenko, A. Zaheri, H. D. Espinosa, M. A. Meyers, *Adv. Mater*. **2019**, *31*, 1804574.

[6] A. Ghazlan, T. Ngo, P. Tan, Y. M. Xie, P. Tran, M. Donough, *Compos. Part B: Eng*. **2021**, *205*, 108513.

[7] D. Sharma, S. S. Hiremath, *Aerosp. Sci. Technol*. **2022**, *127*, 107731.

[8] K. Tai, M. Dao, S. Suresh, A. Palazoglu, C. Ortiz, *Nat. Mater*. **2007**, *6*, 454.

This article is protected by copyright. All rights reserved.

[9] W. Huang, D. Restrepo, J.-Y. Jung, F. Y. Su, Z. Liu, R. O. Ritchie, J. McKittrick, P. Zavattieri, D. Kisailus, *Adv. Mater*. **2019**, *31*, 1901561.

[10] J. Bauer, A. Schroer, R. Schwaiger, O. Kraft, *Nat. Mater*. **2016**, *15*, 438.

[11] H. Ma, J. Hu, P. X. Ma, *Adv. Funct. Mater*. **2010**, *20*, 2833.

[12] M. Alizadeh-Osgouei, Y. Li, C. Wen, *Bioact. Mater*. **2019**, *4*, 22.

[13] S. Deville, E. Saiz, R. K. Nalla, A. P. Tomsia, *Science* **2006**, *311*, 515.

[14] D. Panthi, N. Hedayat, T. Woodson, B. J. Emley, Y. Du, *J. Am. Ceram. Soc*. **2020**, *103*, 878.

[15] T. Hu, M. Shi, X. Zhao, Y. Liang, L. Bi, Z. Zhang, S. Liu, B. Chen, X. Duan, B. Guo, *Chem. Eng. J*. **2022**, *428*, 131017.

[16] R. F. Canadas, T. Ren, A. Tocchio, A. P. Marques, J. M. Oliveira, R. L. Reis, U. Demirci, *Biomaterials* **2018**, *181*, 402.

[17] P. Min, J. Liu, X. Li, F. An, P. Liu, Y. Shen, N. Koratkar, Z.-Z. Yu, *Adv. Funct. Mater*. **2018**, *28*, 1805365.

[18] N. Tian, S. Wu, G. Han, Y. Zhang, Q. Li, T. Dong, *J. Hazard. Mater*. **2022**, *424B*, 127393.

[19] Y. Si, X. Wang, L. Dou, J. Yu, B. Ding, *Sci. Adv*. **2018**, *4*, eaas8925.

[20] A. Gelmi, C. E. Schutt, *Adv. Healthcare Mater*. **2021**, *10*, 2001125.

[21] B. S. Eftekhari, M. Eskandari, P. A. Janmey, A. Samadikuchaksaraei, M. Gholipourmalekabadi, *Adv. Funct. Mater*. **2020**, *30*, 1907792.

[22] T. Hu, M. Shi, X. Zhao, Y. Liang, L. Bi, Z. Zhang, S. Liu, B. Chen, X. Duan, B. Guo, *Chem. Eng. J*. **2022**, *428*, 131017.

[23] E.J. Curry, K. Ke, M.T. Chorsi, K.S. Wrobel, A.N. Miller, A. Patel, I. Kim, J. Feng, L. Yue, Q. Wu, C.L. Kuo, K.W.H. Lo, C.T. Laurencin, H. Ilies, P.K. Purohit, T.D. Nguyen, *Proc. Natl. Acad. Sci. USA*, **2018**, *115*, 909.

[24] Z.-P. Bao, R.-G. Miao, X. Qi, X.-F. Wu, *Chem. Commun*. **2021**, *57*, 1955.

This article is protected by copyright. All rights reserved.

Author Manuscript

[25] G. Tudu, K. S. Paliwal, S. Ghosh, T. Biswas, H. V. S. R. M. Koppisetti , A. Mitra, V. Mahalingam, *Dalton Trans*. **2022**, *51*, 1918.

[26] L. Zhu, S. Chen, K. Liu, W. Wen, L. Lu, S. Ding, C. Zhou, B. Luo, Chem. Eng. J. 2020, 391, 123524.

[27] K. J. Cha, J. M. Hong, D.-W. Cho, D. S. Kim, *Biofabrication* **2013**, *5*, 025007.

[28] J.-S. Lee, H. D. Cha, J.-H. Shim, J. W. Jung, J. Y. Kim, D.-W. Cho, *J. Biomed. Mater. Res. Part A* **2012**, *100A*,1846.

[29] V. J. Chen, P. X. Ma, *Biomaterials* **2004**, *25*, 2065.

[30] V. A. Santamaría, H. Deplaine, D. Mariggió, A. R. Villanueva-Molines, J. M. García-Aznar, J. L. G. Ribelles, M. Doblaré, G. G. Ferrer, I. Ochoa, *J. Non-Cryst. Solids* **2012**, *358*, 3141.

[31] A. J. Cruz-Cabeza, R. J. Davey, I. D. H. Oswald, M. R. Ward, I. J. Sugden, *CrystEngComm* **2019**, *21*, 2034.

[32] Y. G. Ko, P. X. Ma, *CrystEngComm* **2012**, *14*, 7891.

[33] Y. Ha, X. Ma, S. Li, T. Li, Z. Li, Y. Qian, M. Shafiq, J. Wang, X. Zhou, C. He, *Adv. Funct. Mater*. **2022**, *32*, 2200011.

[34] M. Martiniaková, B. Grosskopf, R. Omelka, M. Vondráková, M. Bauerova, *J. Forensic Sci*. **2006**, *51*, 1235.

[35] J. J. Sciote, T. J. Morris, *J. Orthodon*. **2000**, *27*, 15.

[36] R. Lakes, *Nature* **1993**, *361*, 511.

[37] C. Yuan, W. Ji, R. Xing, J. Li, E. Gazit, X. Yan, *Nat. Rev. Chem*. **2019**, *3*, 567.

[38] M. J. Gupte, W. B. Swanson, J. Hu, X. Jin, H. Ma, Z. Zhang, Z. Liu, K. Feng, G. Feng, G. Xiao, N. Hatch, Y. Mishina, P. X. Ma, *Acta Biomater*. **2018**, *82*, 1.

[39] Y. Chen, X. Hu, W. Liu, Theor. *Appl. Fract. Mech*. **2022**, *118*, 103216.

[40] T. Snow, W. Woolley, R. M. Metcalf, J. Rosenberg, C. Acevedo, O. T. Kingstedt*, Int. J. Fract*. **2022**, *233*, 85.

This article is protected by copyright. All rights reserved.

Author Manuscript

[41] M. P. Lutolf, J. A. Hubbell, *Nat. Biotechnol*. **2005**, *23*, 47.

[42] J. D. Hartgerink, E. Beniash, S. I. Stupp, *Science* **2001**, *294*, 1684.

[43] Z. Zhang, R. L. Marson, Z. Ge, S. C. Glotzer, P. X. Ma, *Adv. Mater*., **2015**, *27*, 3947.

[44] V. J. Chen, L. A. Smith, P. X. Ma, *Biomaterials* **2006**, *27*, 3973.

[45] R. Kane, P. X. Ma, *Mater. Today* **2013**, *16*, 418.

[46] D. Chena, J. P. Dunkers, W. Losert, S. Sarkar, *Biomaterials* **2021**, *274*, 120812.

[47] L. A. Smith, X. Liu, J. Hu, P. X.Ma, *Biomaterials* **2010**, *31*, 5526.

[48] Y. Zhang, J. Li, M. Soleimani, F. Giacomini, H. Friedrich, R. Truckenmüller, P. Habibovic, *Adv. Funct. Mater*. **2021**, *31*, 2102911.

[49] K. Kim, D. Dean, A. G. Mikos, J. P. Fisher, *Biomacromolecules* **2009**, *10*, 1810.

[50] C. E. Holy, M. S. Shoichet, J. E. Davies, *J. Biomed. Mater. Res*. **2000**, *51*, 376.

[51] G. B. Wei, P. X. Ma, *Biomaterials* **2004**, *25*, 4749.

Author Manuscript

This article is protected by copyright. All rights reserved.

Author Manuscript

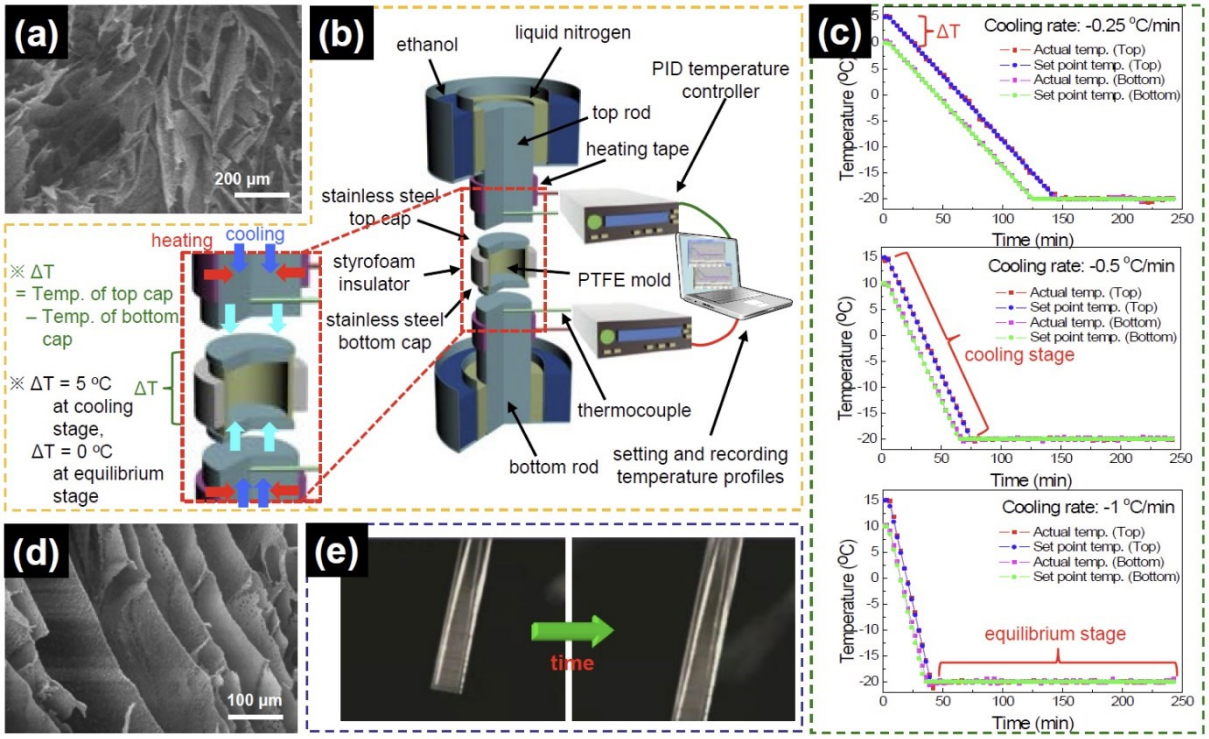


Figure 1. Directional freezing apparatus and oriented scaffold architectures. (a) SEM image of a PLLA scaffold with randomly-oriented pores fabricated at -20 °C in a freezer. (b) Schematic of the apparatus to directionally freeze the polymer solution. (c) Freezing temperature-time profiles of two metal rods with cooling rates of -0.25 °C/min, -0.5 °C/min, and -1 °C/min. (d) SEM image of the lamellar PLLA scaffold fabricated at the cooling rate of -1 °C/min. (e) Representative still images of the plate-like crystal structure of DMC from a movie file (Movie S1, Supporting Information). The growth of the plate-like DMC crystals was observed as the freezing time of DMC vapor was increased.

This article is protected by copyright. All rights reserved.

Author Manuscript

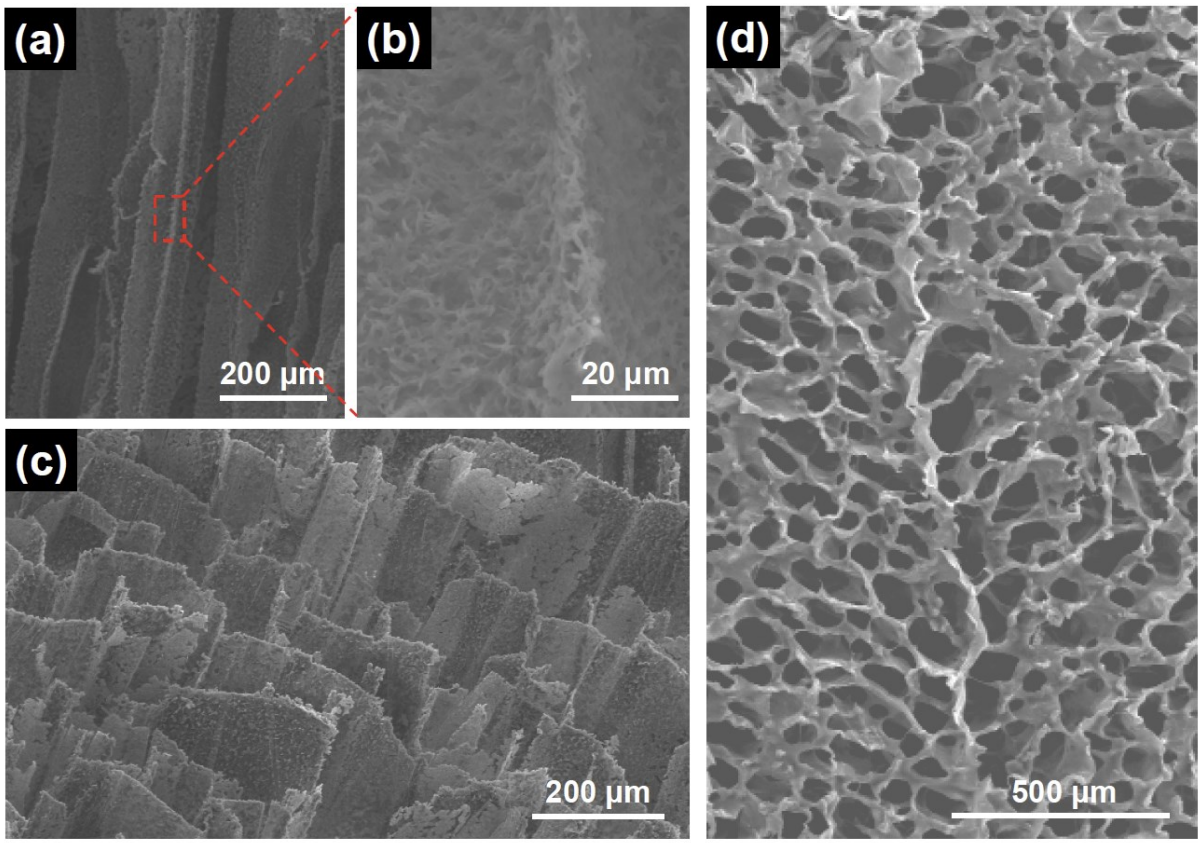


Figure 2. Preparation of honeycomb-mimic PLLA scaffolds. (a), (c) and (d) SEM images of the honeycomb-mimic PLLA scaffolds fabricated at the cooling rate of -1 ^{o}C min^{-1} (a: longitudinal view, c: diagonal view, and d: cross-sectional view). (b) SEM image of high magnification of dotted square in Figure. 2a.

This article is protected by copyright. All rights reserved.

Author Manuscript

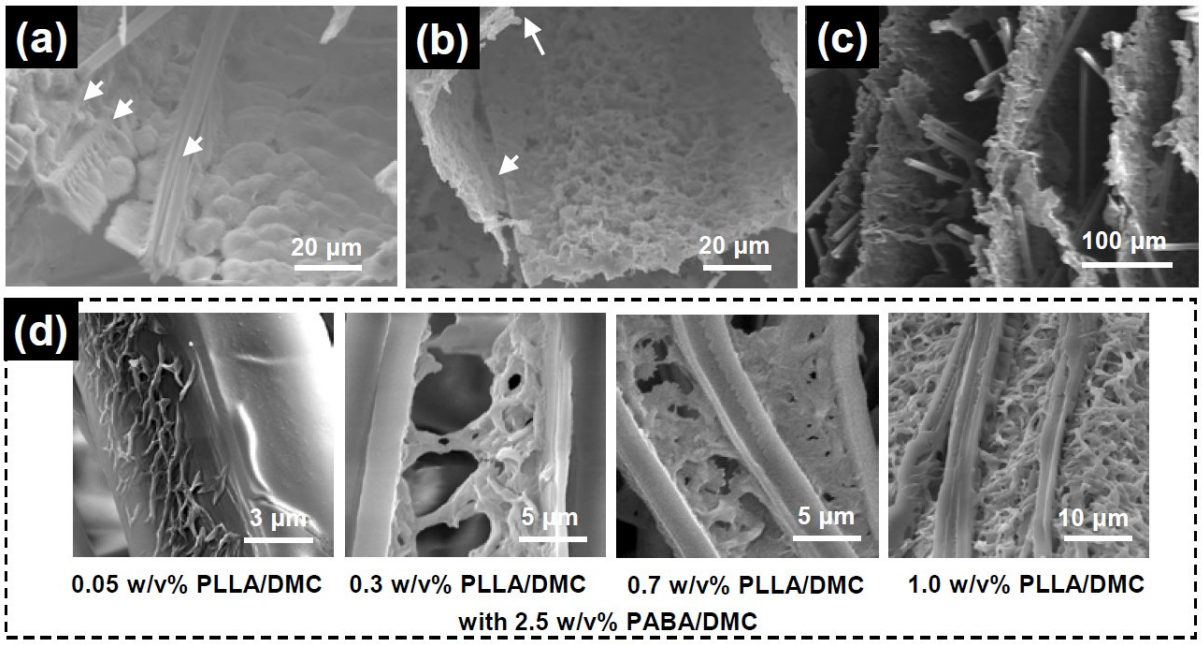


Figure 3. The data and illustration of the role of PABA crystal growth in phase-separation and scaffold architecture formation. SEM images of the PLLA tubules (a) before leaching PABA and (b) after leaching PABA. Arrows indicate (a) PABA crystals and (b) vestiges of PABA crystals. (c) PLLA scaffold fabricated with 2.5% (w v^{-1}) PLLA and 2.5 % (w v^{-1}) glass fibers in DMC at the cooling rate of -1 °C min^{-1}. (d) The PLLA wall formation between PABA crystals was examined as a function of PLLA concentration.

This article is protected by copyright. All rights reserved.

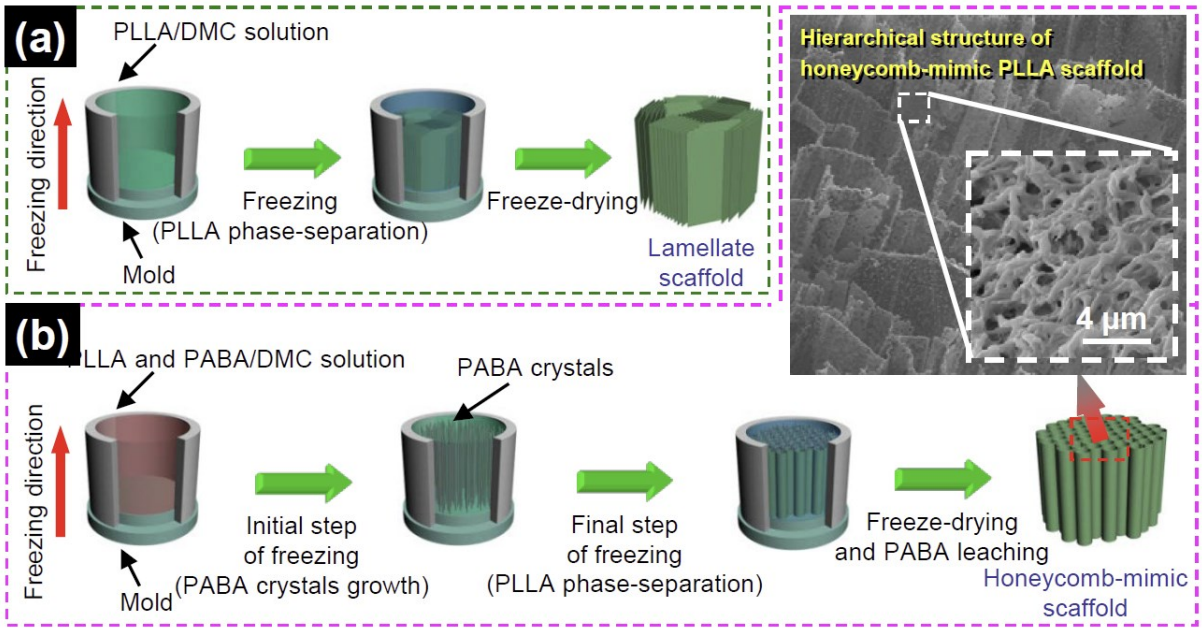


Figure 4. Illustration of the scaffold architecture formation. (a) When PLLA/DMC solution was used to fabricate the lamellar PLLA scaffolds, the DMC should have nucleated on the bottom of the mold and the plate-like crystals grew along the freezing direction to the top of the mold, resulting in the formation of layered PLLA walls that were originally sandwiched between DMC crystals. (b) However, the existence of PABA in the PLLA/DMC solution should have resulted in a two-step crystallization process. Needle-shaped PABA crystals should have formed in the first step prior to the DMC crystallization. These in situ formed PABA crystal needles likely served as the substrate at the bottom of the mold to induce the DMC crystallization along two opposite sides of the PABA fibers as two parallel crystal plates growing from the bottom to the top. The growth of the two crystallized DMC plates on the two opposite sides of a PABA crystal needle concentrated the PLLA in between. This process led to the formation of a PLLA wall along the freezing direction (vertical direction). The PLLA wall met with another PLLA wall or a needle-like PABA crystal, leading to the formation of a corner edge of a tubule along the freezing direction. Due to the growth of many PABA needles and therefore many PLLA walls, honeycomb PLLA tubules were formed. The fabricated honeycomb-mimic scaffold exhibited a hierarchical structure from nanofibers to micro-/macro-tubular structures.

This article is protected by copyright. All rights reserved.

Author Manuscript

Author Manuscript

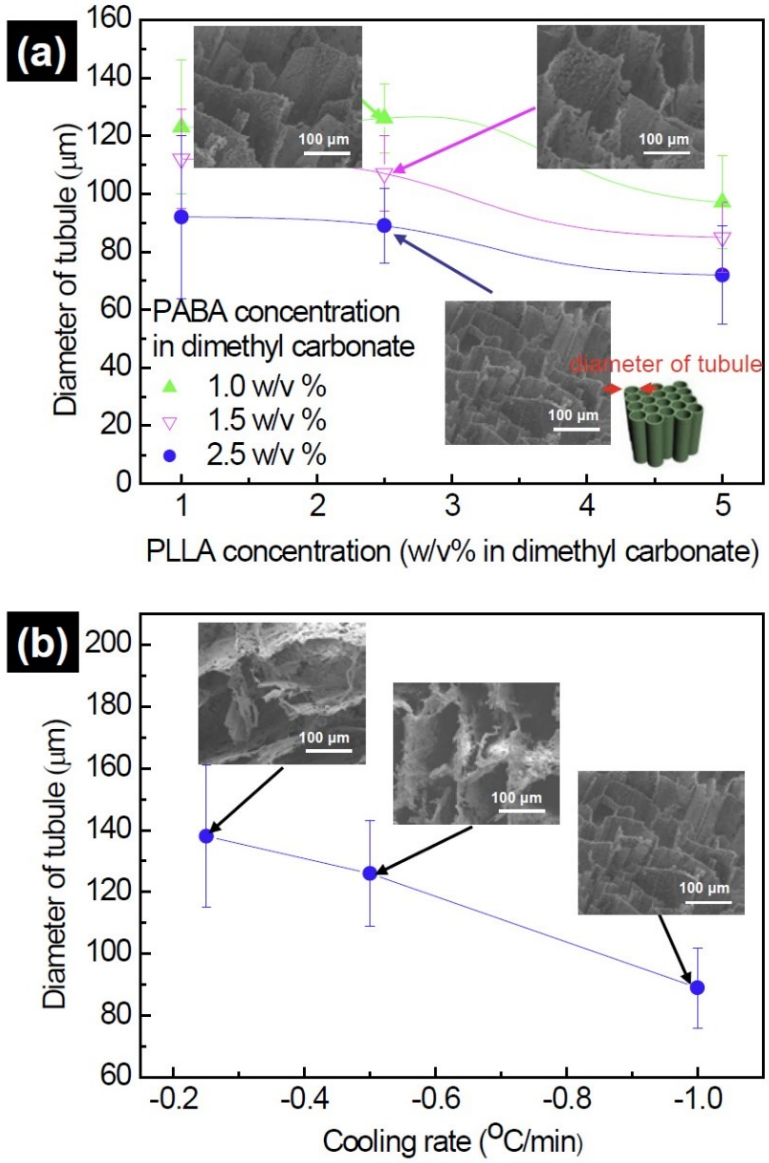


Figure 5. Effect of concentration and cooling rate on the diameter of the tubules. (a) The diameter of tubules in the PLLA scaffold fabricated at various PLLA and PABA concentrations. All scaffolds were fabricated at the cooling rate of -1 °C min^{-1}. (b) The diameter of tubules in the PLLA scaffolds fabricated at various cooling rates. All scaffolds were fabricated at the concentration of 2.5% (w v^{-1}) PLLA and 2.5% (w v^{-1}) PABA.

This article is protected by copyright. All rights reserved.

Author Manuscript

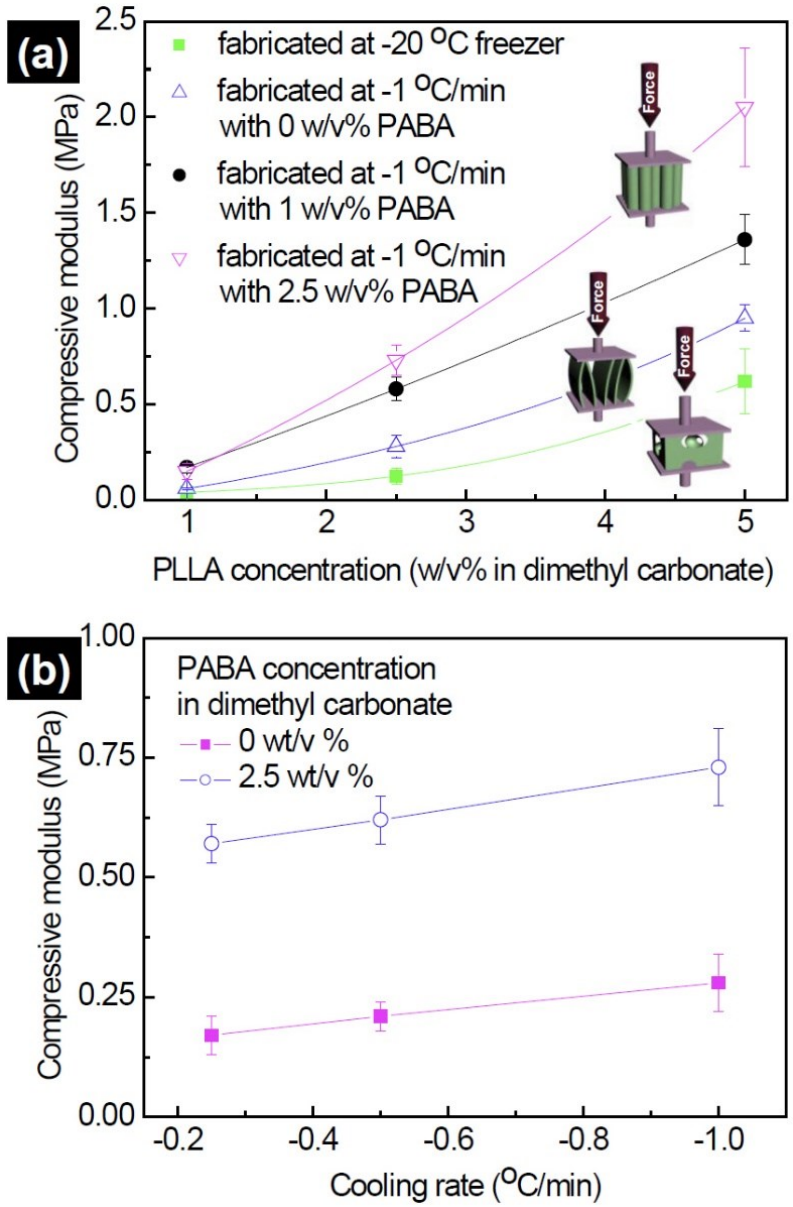


Figure 6. Effect of concentration and cooling rate on compressive modulus against vertical loading. (a) Compressive modulus of the PLLA scaffold fabricated at various PLLA and PABA concentrations. (b) Compressive modulus of the PLLA scaffold fabricated at various cooling rates and PABA

This article is protected by copyright. All rights reserved.

concentrations. All scaffolds were fabricated at the concentration of 2.5% (w v^{-1}) PLLA. The load was applied in the direction parallel to the tubular axis or the polymer layer planes to measure the compressive modulus.

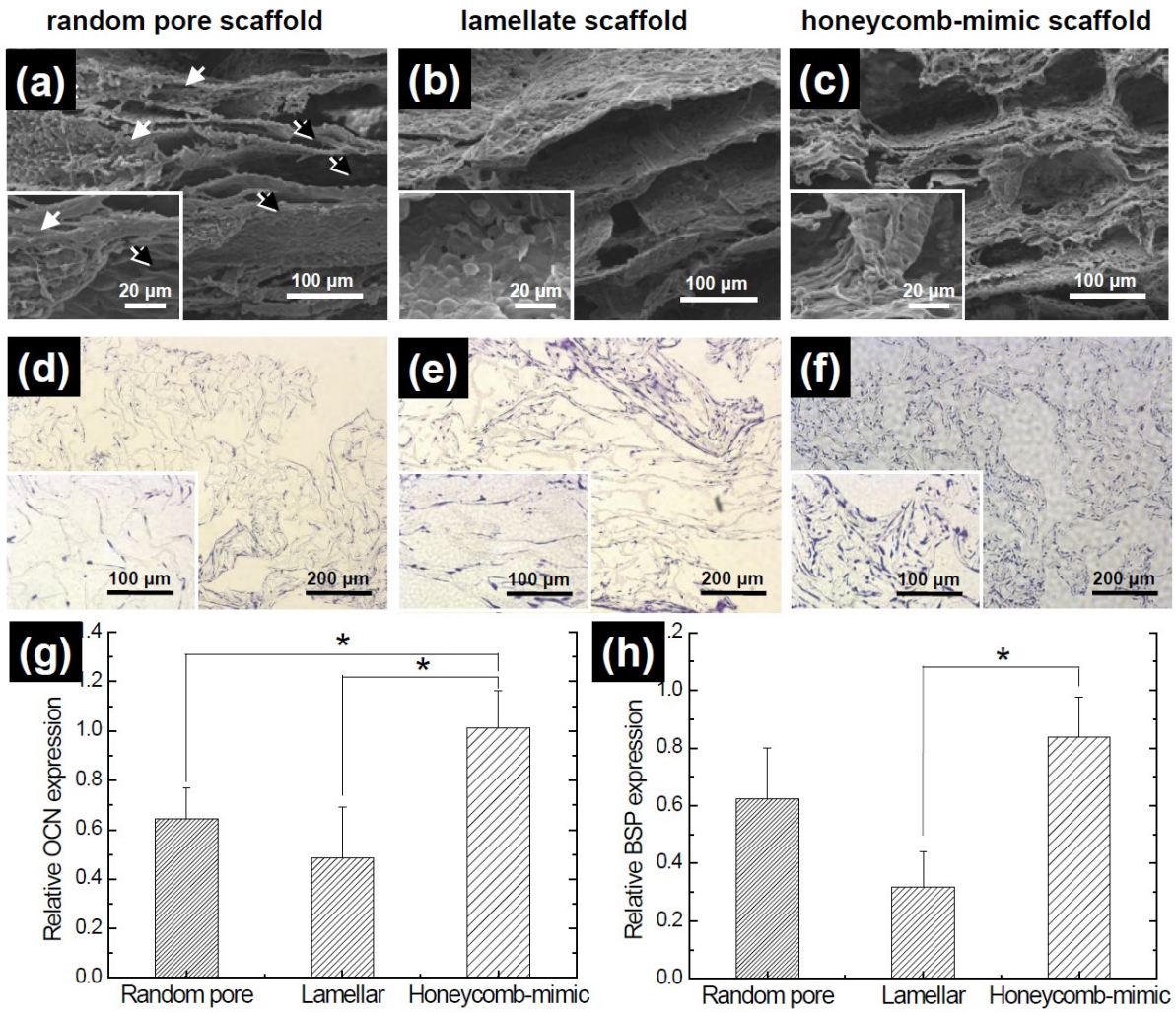
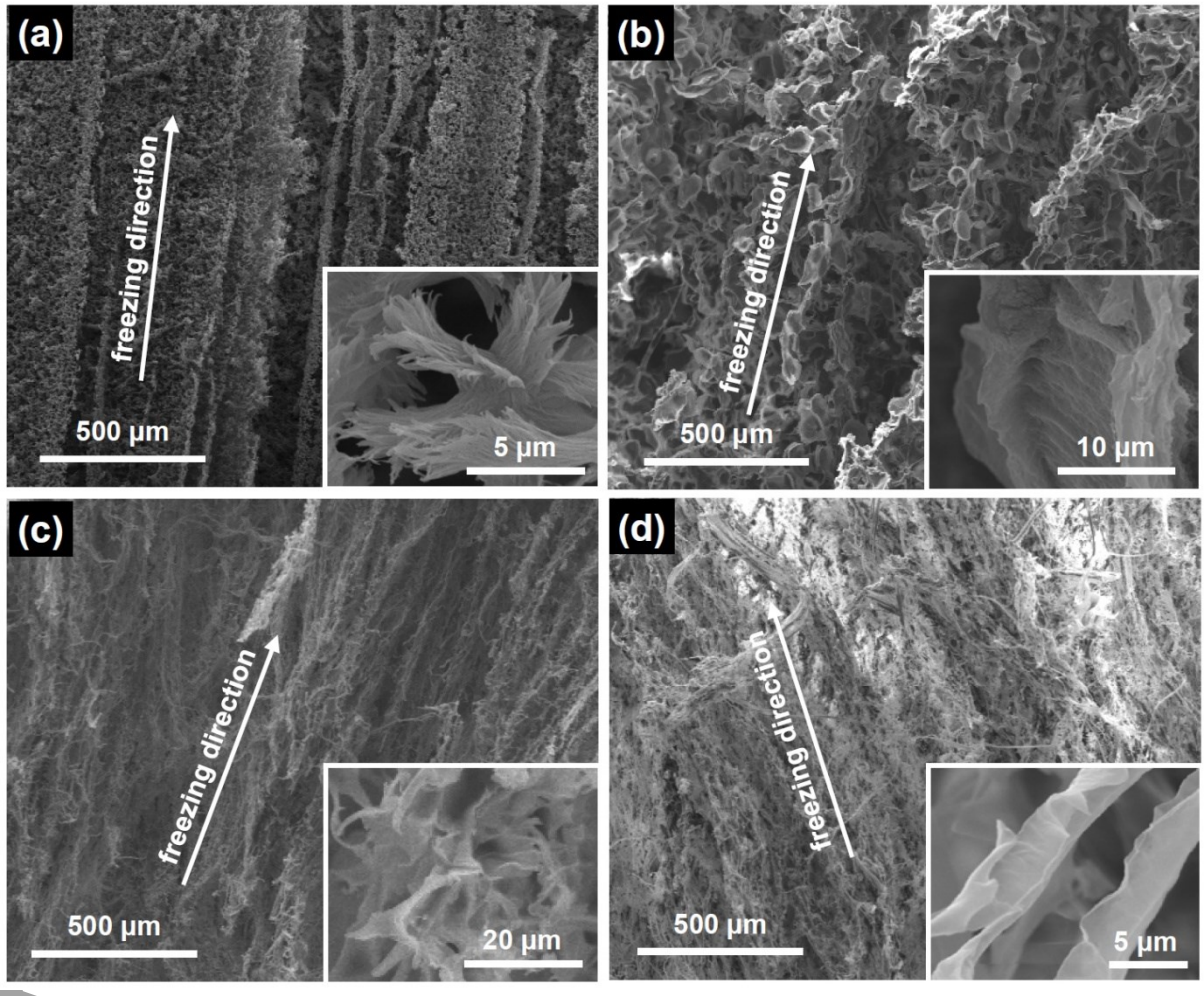


Figure 7. *In vitro* performance of PLLA scaffolds after being seeded with MC3T3-El osteoblasts. SEM images of (a) PLLA scaffold with random pores, (b) lamellar PLLA scaffold, and (c) honeycomb-mimic PLLA scaffold 3 days after cell seeding. White arrows and black arrows denote cells-adhered regions

This article is protected by copyright. All rights reserved.

and not cells-adhered regions in the PLLA scaffold with random pores, respectively. H&E staining images of the cross sections of (d) PLLA scaffold with random pores, (e) lamellar PLLA scaffold, and (f) honeycomb-mimic PLLA scaffold after cell seeding and cultured under differentiation conditions for 2 weeks. Relative levels of bone marker expression in PLLA scaffolds after 2 weeks of culture under differentiation conditions; (g) osteocalcin (OCN) expression, and (h) bone sialoprotein (BSP) expression (* indicates $P < 0.05$).



Author Manuscript

This article is protected by copyright. All rights reserved.

Figure 8. SEM images of PLLA scaffolds fabricated using the co-solvent system and the unidirectional-freezing apparatus (PLLA concentration: 2.5% (w v^{-1}), cooling rate: -1 ^{o}C min^{-1}). (a) DMC/EtOH (v:v) = 8:2, (b) DMC/THF (v:v) = 7:3, (c) DMC/1,4-dioxane (v:v) = 1:1, and (d) 1,4-dioxane/benzene (v:v) = 1:1. Insets exhibit the wall textures of the each scaffold.

A novel method for the fabrication of the honeycomb-mimic PLLA scaffold by crystal needle-guided directional phase separation is presented. The fabricated honeycomb-mimic scaffold shows a hierarchical architecture from nano- to macro-scale with nanofibrous walls. The differentiation of MC3T3-E1 pre-osteoblastic cells is enhanced on the honeycomb-mimic PLLA scaffold.

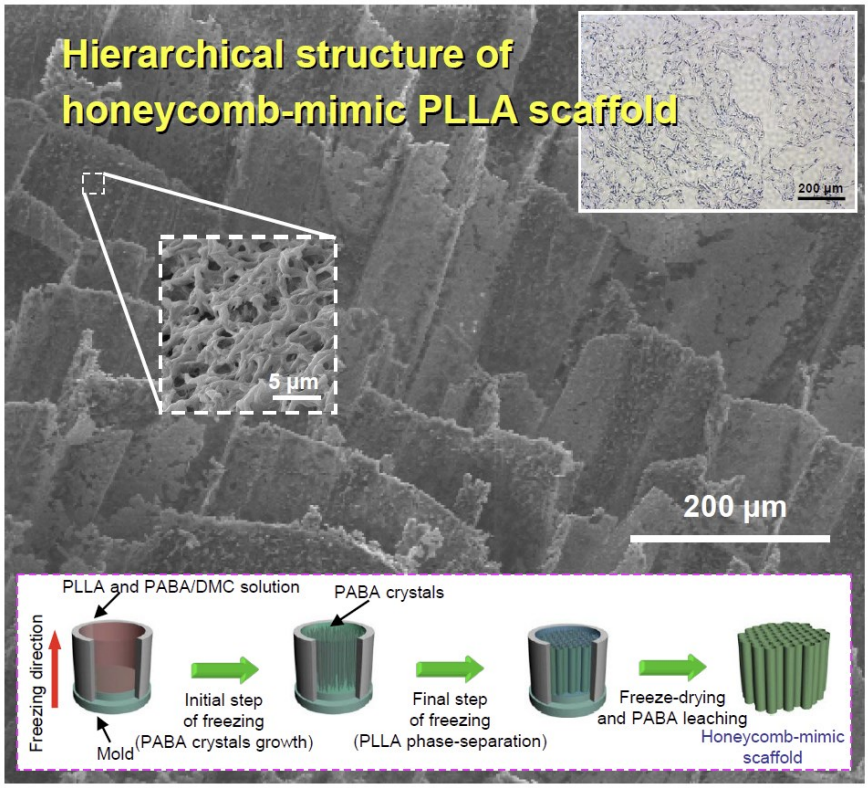
Y. G. Ko,* L. A. Smith Callahan, P. X. Ma*

Biodegradable Honeycomb-Mimic Scaffolds Consisting of Nanofibrous Walls

Author Manuscript

This article is protected by copyright. All rights reserved.

Author Manuscript



This article is protected by copyright. All rights reserved.